Fibrinogen, Collagen and Transferrin Adsorption to PEDOT-XRU glycan composite Conducting Polymer Biomaterials for Wound Healing Applications

Running title: PEDOT-XRU glycan composite Conducting Polymer Biomaterials

Running Authors: Molino et al.

Paul J Molino[a)]*

ARC Centre of Excellence for Electromaterials Science (ACES), Intelligent Polymer Research Institute, University of Wollongong, Wollongong, Australia

John Will

Department of Bioengineering, The University of Texas at Dallas, Richardson, TX, USA

Luciana Yumiko Daikuara

ARC Centre of Excellence for Electromaterials Science (ACES), Intelligent Polymer Research Institute, University of Wollongong, Wollongong, Australia

Alexander R Harris

ARC Centre of Excellence for Electromaterials Science (ACES), Department of Medicine, Dentistry and Health Sciences, University of Melbourne, Melbourne, Australia

Zhilian Yue

ARC Centre of Excellence for Electromaterials Science (ACES), Intelligent Polymer Research Institute, University of Wollongong, Wollongong, Australia

Jeremy Dinoro

ARC Centre of Excellence for Electromaterials Science (ACES), Intelligent Polymer Research Institute, University of Wollongong, Wollongong, Australia

Pia Winberg

Venus Shell Systems Pty. Ltd, 220 Bolong Rd, Bomaderry, Australia

Gordon G Wallace[b)]*

ARC Centre of Excellence for Electromaterials Science (ACES), Intelligent Polymer Research Institute, University of Wollongong, Wollongong, Australia

a)Electronic mail: pmolino@uow.edu.au

b)Electronic mail: gwallace@uow.edu.au

We present the conducting polymer poly (3,4-ethylenedioxythiophene) (PEDOT) doped with an algal derived glycan-extract, Phycotrix™ (XRU84), as an innovative electrically conductive material capable of providing beneficial biological and electrical cues for the promotion of favourable wound healing processes. Increased loading of the algal xylorhamno-uronic glycan (XRU84) into PEDOT resulted in reduced surface nanoroughness and polymer shear modulus, and increased static water contact angle. PEDOT- XRU84 films demonstrated good electrical stability and charge storage capacity, and reduced impedance relative to the control gold electrode. QCM-D study of protein adsorption (transferrin, fibrinogen, collagen) showed collagen adsorption increased significantly with increased XRU84 loading, while transferrin adsorption was significantly reduced. The viscoelastic properties of adsorbed protein, characterised using the $\Delta D/\Delta f$ ratio, showed that for transferrin and fibrinogen a rigid, dehydrated layer was formed at low XRU84 loadings. Cell studies using Human Dermal Fibroblasts demonstrated excellent cell viability, with fluorescent staining of the cell cytoskeleton illustrating all polymers to present excellent cell adhesion and spreading after 24 hrs.

I. INTRODUCTION

Wound healing is a complex biological process that requires numerous biological processes and pathways to be engaged in a synchronised way in order to repair and/or regenerate damaged tissues[1]. Application of conductive materials in wound healing relates to a capacity for accelerating cell proliferation and migration, improving anti-bacterial properties, and regulation of the delivery of growth factors that can direct the process of wound healing towards that of functional tissue[2]. Regardless of the injury site or

he type of tissue damaged, the wound healing process is remarkably similar, involving inflammation, new tissue formation, and tissue remodelling[1, 3-4]. The newly formed tissue may be formed either through fibrosis, which results in non-functional tissue, or regeneration which produces tissue which restores the functionality of the original tissue. Wound healing following the fibrosis pathway results in significant economic burden, with diseases resulting from fibrosis believed to cost tens of billions of dollars annually[1], notwithstanding the significant social implications that can result in lifelong disability for patients[5].

In general, modern materials for wound healing applications can be categorised based on their mode of action (passive, interactive or bioactive)[6]. Passive wound healing materials that include gauze, lint, and cotton wool provide excellent gas exchange, remove exudate and prevent contamination of the wound site[7]. Interactive materials, including foam, hydrocolloids (i.e. gelatin, carboxymethylcellulose) and hydrogels (i.e. glycerine, alginate), can act to either dry or moisten the wound site, are more malleable and therefore contour better with the geometry of the injury site, and can easily be incorporated with antimicrobials such as silver to reduce the risk of infection[4, 8-11]. Bioactive dressings incorporate components that play an active role in the healing process. These materials may include extracellular matrix components such as collagen[12] and hyaluronic acid[13], and are designed to directly interface with the injured tissues, providing a biosynthetic bandage to support cell proliferation and chemotaxis[14]. However, it has become evident that for most applications, a single dressing type will not sufficiently address all of the requirements for the wound healing process[6]. Furthermore, it has become highly desirable to have a wound healing material that can interact directly with the wound and provide various physical, chemical, mechanical and even electrical stimuli to promote tissue repair[15-17]. As

such significant research is currently focused on developing the next generation of multifunctional wound healing materials.

Much development has been directed to composite wound dressing biomaterials that combine both synthetic and biologically derived materials and can provide a material that promotes several processes required to enhance the body's natural healing and regenerative capacity at the wound site. Conducting polymers are one class of materials that have attracted particular interest in wound healing due to their inherent cytocompatibility, and their capacity to deliver specific chemical, electrical and mechanical stimuli to cells and tissues[18-22]. However there remain challenges regarding our ability to control and tailor how conducting polymers interface with the biological environment. Our ability to tune polymer properties, such as chemistry, wettability, modulus, and conductivity, is critical to enhancing interactions with cells and tissues. In particular, it is vital to ensure appropriate interfacing between the polymers and proteins that play a crucial role in mediating cell – material adhesion[23-25], as well as guiding various cell processes, including those critical to wound healing, such as cell migration[25]. Proteins known to be particularly critical in mediating these interactions include fibrinogen and collagen, both important extracellular matrix proteins[26-27], and transferrin, an iron binding and transport blood plasma glycoprotein that plays a role in angiogenesis[28]. Researchers have sought to control protein – polymer interactions by using polymer electrochemical properties[23-24, 29], as well as modulating polymer surface properties (nanoroughness, wettability)[23, 30], and through the identity of the dopant species[31-32]. In particular, the use of biological, as opposed to synthetic, dopants is seen as an appealing avenue through which to enhance biological interactions with the polymeric materials.

Conducting polymers have been explored as tissue engineering conduits for neural[19, 33] and muscle[34] regeneration, and for controllable release of various drugs and growth factors[35-36]. Polypyrrole composite films with biological dopants such as heparin[37] and hyaluronic acid[38] have been demonstrated to present desirable properties for wound healing, with electrical stimulation of fibroblast cells shown to enhance cell proliferation and migration[39] as well as upregulation of genes relevant to wound healing[40]. However few studies have investigated the use of the conducting polymer Poly (3,4-ethylenedioxythiophene) (PEDOT) for wound healing applications[24, 41]. PEDOT is attractive for biomedical applications due to its chemical stability, and its relatively soft mechanical nature and high degree of hydration, thus conforming more closely with biological tissue and the extracellular environment relative to other cytocompatible conducting polymers. Those studies that have used PEDOT for wound healing have only incorporated synthetic dopants, such as tosylate and polystyrene sulphonate[24-25, 41]. In this study we explore the development of PEDOT doped with the biological dopant XRU as a new smart biomaterial for wound healing applications. XRU is a naturally occurring highly sulphated polysaccharide produced by a particular species of marine green macroalga from the ulvacean family. It is found to possess a wide distribution of molecular weights and charge densities[42] and even monomer composition is species dependent. Sulphated, macroalgal XRU has attracted interest in the field of biomaterials science due to its biochemical similarity to mammalian glycans such as heparin, heparin sulphate, chondroitin sulphate and dermatan sulphate[43]. The characteristics and biological functionality are dependent on the sources, but broadly XRU has demonstrated biochemical properties such as anticoagulant[44], anti-inflammatory and antibacterial properties[45] . It also provides structural biomimicry of extracellular matrix function with excellent cell attachment[46] and enhanced protection of matrix proteins such as collagen[47].

The sourcing of a biofunctional material from algae is seen as an enormous advantage that will provide a cheap, reliable and highly scalable source of material that does not present ethical concerns regarding animal derived materials, or the potential spread of associated pathogens.

We have previously constructed electrochemically polymerised polymeric films of PEDOT-XRU, and demonstrated enhanced biocompatibility and neuronal cell differentiation[32]. Here we use different concentrations of XRU type polymer from an Australian sourced species of *ulvaceae* (chlorophyta)), (Phycotrix™ (XRU84), provided by Venus Shell Systems Pty Ltd (MW ~ 1,100,000 and >50% rhamnose[46]), to prepare PEDOT composites. We characterise the physical, mechanical and electrochemical properties of materials prepared using differing concentrations of XRU84 in the polymerisation electrolyte. The ability for the PEDOT-XRU films to interface with the proteins collagen, transferrin and fibrinogen, that play an important role in wound healing processes was investigated. We also undertake initial cell biocompatibility and interfacing studies using human dermal fibroblasts as a model to inform on the materials use in wound healing applications.

II. EXPERIMENTAL

A. Materials

3,4-Ethylenedioxythiophene (EDOT) was purified via distillation and stored at -18 °C. Transferrin and fibrinogen proteins were purchased from Sigma Aldrich (Sydney Australia), and bovine collagen protein purchased from Invitrogen, with all stored at 4 °C prior to use. All other reagents were purchased from commercial houses and used as received. The XRU rich glycan, Phycotrix™ (XRU84), was provided by Venus Shell Systems Pty. Ltd. (VSS, Australia).

B. Electrochemical Polymerisation of PEDOT- XRU84 Films

Electrochemical polymerisation of EDOT was performed using a Q-Sense Electrochemistry Module (QEM 401) flow cell with a Q-Sense E4 Quartz Crystal Microbalance system (Q-Sense AB, Västra, Frölunda, Sweden). The QCM-D sensor was an A-T cut quartz crystal with a 10 mm diameter gold electrode (QSX301) with a fundamental resonance frequency of 5 MHz (Q-Sense AB, Västra, Frölunda, Sweden). Prior to polymerisation, the Au electrode surface was cleaned with piranha solution (3:1 solution of sulfuric acid: hydrogen peroxide) for 3 mins, followed by thorough rinsing with deionised water and dried under nitrogen gas. Aqueous solutions of EDOT were prepared consisting of 0.01 M EDOT in deionised water with either 0.2, 2 or 20 mg/ml^{-1} of XRU84 added to form the polymerisation electrolyte. Each solution was de-oxygenated via bubbling with nitrogen gas for 10 mins prior to use. PEDOT-XRU84 polymer films were polymerised using an eDAQ e-corder 410 recorder and an EA163 potentiostat coupled with the QEM 401 electrochemistry module. The QEM 401 electrochemistry module consisted of a platinum counter electrode, an Ag|AgCl reference electrode, and the Au electrode on the QCM sensor as the working electrode. The aqueous EDOT-XRU84 solution was passed through the QEM 401 flow module at a rate of 60 µl min^{-1}, and once the QCM frequency and dissipation parameters were stable, a 0.25 mA cm^{-2} current density was applied for 2 mins for each polymer film growth (total charge of 0.03 C cm^{-2}). After polymerisation the quartz electrodes supporting the polymerised films were removed from the QEM 401 flow cell, rinsed with deionised water and dried under nitrogen gas.

C. PEDOT-XRU84 Film Characterisation

1. Atomic force microscopy

The morphology of the polymer films surfaces was imaged using a MFP-3D atomic force microscope (AFM) (Asylum Research, CA) with a Mikromasch NSC15 cantilever (spring constant ~37 N m^{-1}). Images of dry films were obtained in AC mode (5 µm x 5 µm) at a scan rate of 0.5 Hz in air. The Asylum Research Analysis software with the Igor Pro Software Package (WaveMetrics, OR) was used to determine the RMS roughness and surface area values.

2. Goniometry

Static water contact angle measurements were performed using a DataPhysics optical contact angle goniometer. At least 3 measurements were undertaken on 3 separate films using deionised water droplets of 2 µl for each reported value.

3. Profilometry

The thickness of the PEDOT-XRU84 polymer films was determined using a stylus profilometer (Veeco Dektak 150 Stylus Profilometer). PEDOT-XRU84 films were polymerised on chromium (3 nm) and gold (50 nm) sputter coated coverslips, using the same polymerisation conditions described for the QCM studies (i.e. 0.25mA.cm^{-2} current density for 2 mins). A scratch was then gently etched into the polymer film, and the thickness of the PEDOT-XRU films recorded for films polymerised with the different concentrations of the electrolyte (0.2mg/ml^{-1}, 2 mg/ml^{-1}, 20 mg/ml^{-1} XRU84) used to provide the dopant.

4. Quartz Crystal Microbalance with Dissipation Monitoring (QCM-D) Modelling of Polymer Mass and Shear Modulus

In-situ measurement of QCM-D parameters during film polymerisation allowed detailed analyses of the physical properties of the various PEDOT-XRU84 polymer films. The Q-tools software package was used to apply the Voigt model to determine layer mass and shear

modulus. Polymer density was determined using the polymer mass calculated by initially modelling the QCM-D data, and profilometry thickness data. For polymer density, the following values were calculated and used for the modelling of polymer thickness and shear modulus: 3,105 kg/m^3 (0.2mg/ml^{-1} XRU84); 1,306 kg/m^3 (2 mg/ml^{-1} XRU84) and 1,136 kg/m^3 (20 mg/ml^{-1} XRU84). The Voigt model was then used to calculate polymer shear modulus using the following input parameters that provided the best data fit were 1020 kg m^{-3} (fluid density), 0.0001 ≤ 20 kg ms^{-1} (layer viscosity), 10 000 ≤ 1^{10} Pa (layer shear modulus), and 1^{-9} ≤ 1^{-6}m (thickness).

5. Cyclic Voltammetry and Impedance Spectroscopy

Electrochemical experiments were performed on a CHI660E potentiostat (CH Instruments). Electrodes were tested in a 3-electrode configuration using a Ag/AgCl (3 M KCl) as reference electrode and Pt wire as counter electrode. The test solution was PBS that was degassed with nitrogen for at least 10 minutes. Cyclic voltammetry was performed with a potential window of 0.8 to -0.8 V at a scan rate of 100 mV s^{-1}. The charge storage capacity was measured from the second cycle by transforming the current-potential plot to a current-time plot and integrating the reduction and oxidation sweeps separately. Electrochemical impedance spectroscopy (EIS) was performed at 0 V with an AC amplitude of 5 mV over a frequency range of 1-100,000 Hz. Equivalent circuit fitting of the EIS data was performed with ZView (Scribner Associates).

6. Quartz Crystal Microbalance Characterisation of Protein Adsorption to PEDOT- XRU84 Polymer Films

Protein adsorption experiments were carried out using a Q-Sense E4 Quartz Crystal Microbalance system (Q-Sense AB, Västra, Frölunda, Sweden). QCM sensor electrodes with

the polymerised PEDOT- XRU84 film were transferred to a standard Q-Sense flow module (QFM 401) and equilibrated in PBS at 22 °C until stable frequency and dissipation values were established. Experiments were carried out at 22 ± 0.02 °C for the duration of the experiment. Following equilibration, either a 50 µg mL^{-1} solution of collagen, a 50 µg mL^{-1} of transferrin or a 1 mg/ml^{-1} of fibrinogen in PBS at physiological pH (7.4) was introduced into the axial flow module at a flow rate of 10 µl min^{-1} for 60 min, and then rinsed with PBS at a rate of 10 µl min^{-1} for 40 mins or until the QCM measurement parameters stabilised. All experiment were run in triplicate.

The Q-Tools software package was used to apply the Voigt model to determine the mass (ng cm^{-2}) of the viscoelastic protein adlayer. The model input parameters that provided the best data fit were 1150 kg m^{-3} (layer density), 1020 kg m^{-3} (fluid density), $1^{-6} \leq 1^{-2}$ kg ms^{-1} (layer viscosity), $1^4 \leq 1^7$ Pa (layer shear modulus), and $115 \leq 1.15^5$ ng cm^{-2} (mass). The 3rd, 5th and 7th overtones were used for all modelling calculations. The QCM-D modelled mass values refer to the hydrated protein mass adsorbed to the polymer surface. Therefore adsorbed mass (Δm) refers to contributions from both the protein and water hydrodynamically coupled, or trapped, with the protein molecules.

D. Cell Viability and Morphology Studies

1. Cell Culture

Human dermal fibroblasts (HDFs) (Cell Applications) were cultured in Dulbecco's Modified Eagle Medium (DMEM, high glucose, HEPES (Sigma-Aldrich)) supplemented with 10% v/v fetal bovine serum (FBS), 1% v/v penicillin/streptomycin (P/S) under standard culture conditions in a humidified atmosphere with 5% CO_2 at 37°C.

2. Cell Viability and Morphology Studies on PEDOT-XRU84 Films

Films were placed in 12 well plates and incubated overnight in culture media under standard culture conditions before cell seeding. HDF passage 9 were seeded at density of 20,000 cells/cm^{-2} and samples were collected after 2h and 24h. For the evaluation of cell viability, LIVE/DEAD assay was performed using calcein AM (5 µg/ml^{-1}) / propidium iodide (PI, 1 µg/ ml^{-1}) (Life Technologies) and imaged using a confocal laser scanning microscope (Leica TSC SP5 II). ImageJ was used to quantify the number of total live and dead cells within the samples (n > 8). One-way analysis of variance (ANOVA) test followed by Tukey's post-hoc test was used to assess the statistical significance of results between groups. The statistical analysis was performed with the software OriginPro at a confidence level of 95%. Differences were considered statistically significant at $p < 0.05$. Data were expressed as the mean ± standard deviation (SD) for n > 3. Phalloidin staining was used to observe changes in cell morphology. Samples were stained with Alexa Fluor 488 phalloidin (5:200) (Life Technologies) in 5% v/v donkey serum for 1 hour and counterstained with 4',6-di-amidino-2-phenylindole dihydrochloride (DAPI, 1 µg/ ml^{-1}) diluted in 5% v/v donkey serum (Life Technologies) for 10 minutes and imaged using a confocal laser scanning microscope (Leica TSC SP5 II).

III. RESULTS AND DISCUSSION

A. PEDOT-XRU84 Film Characterisation

1. Topography, Morphology and Modulus

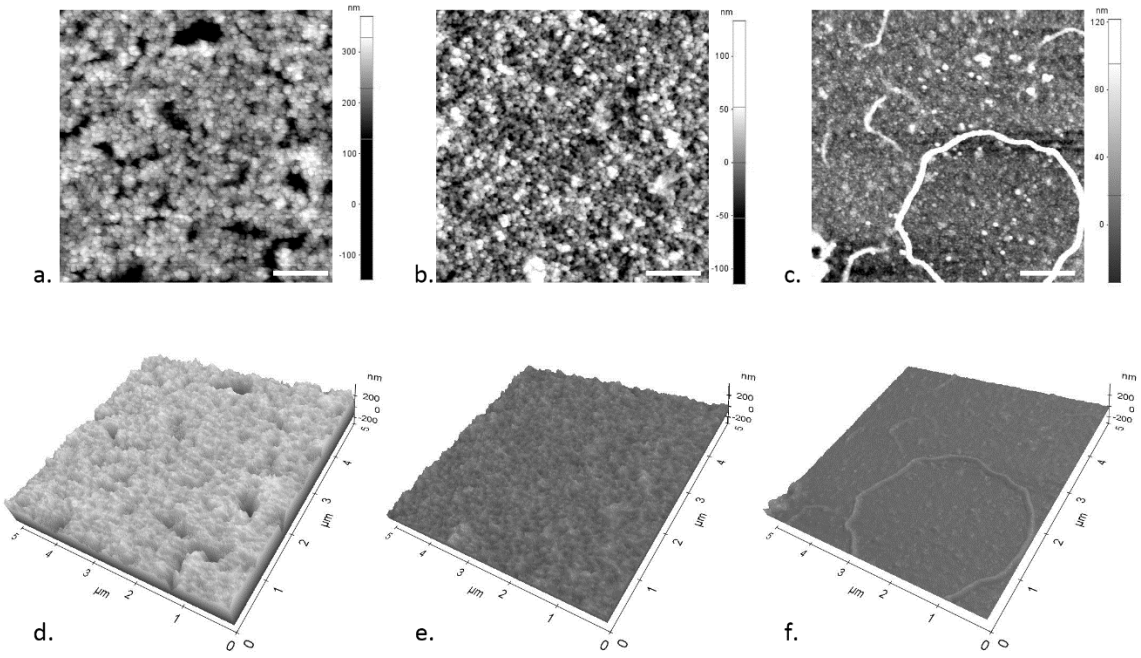

FIG 1. 2D (a-c) and 3D (d-f) representative Atomic Force Microscopy images of the PEDOT-XRU films polymerised with 0.2 mg/ml $^{-1}$ (a,d), 2 mg/ml $^{-1}$ (b,e) and 20 mg/ml $^{-1}$ (c,f) XRU concentration in the polymerisation electrolyte. Scale bars for a-c represent 1µm.

Three different variants of PEDOT-XRU84 polymer films were produced based on the XRU84 electrolyte concentration during polymerisation, providing different degrees of XRU84 loading into the polymer films. Hereafter these different films will be referred to based on their XRU84 bioloading conditions during polymerisation, being 0.2 mg.ml^{-2}, 2 mg.ml^{-2} and 20mg.ml^{-2}. PEDOT-XRU84 films polymerised with XRU84 concentrations of 0.2 mg.ml^{-2} exhibited a nodular surface morphology that is characteristic of electrochemically polymerised PEDOT films, particularly those doped with large biomolecular dopants[48]. Polymer surface roughness was negatively correlated with the XRU84 electrolyte concentration in the polymerisation solution, with RMS roughness increasing ~ 5-fold with a decrease in the XRU84 electrolyte concentration from 20 mg/ml^{-1} to 0.2 mg/ml^{-1} (Table 1). The increase in surface roughness saw a concomitant increase in interfacial surface area.

Polymer mass was negatively correlated with XRU84 bioloading, while polymer thickness was comparable between the 0.2mg/ml^{-1} and 2 mg/ml^{-1} bioloaded films, with the 20mg/ml^{-1} films shown to be significantly thinner. The polymer shear modulus was also similar between the 0.2mg/ml^{-1} and 2mg/ml^{-1} XRU84 loaded films, but was considerably less for the 20mg/ml^{-1} PEDOT-XRU84 composite, while increasing XRU84 concentration in the polymerisation solution also resulted in an increase in the polymer hydrophilicity (table 1).

Previous studies have shown that reducing the concentration of large polyanion dopants in the polymerisation solution results in an increase in the surface roughness of electrochemically polymerised polypyrrole films[49]. In one study electrochemically polymerised PPy doped with the biological dopant dextran sulphate using comparable concentrations of the dopant in the polymerisation electrolyte (0.2, 2 and 20 mg/ml^{-1}) revealed similar effects on polymer properties, with polymer mass and thickness decreasing as a function of increasing dopant concentration during polymerisation[49]. PPy films polymerised with 0.2 mg/ml^{-1} DS concentration were shown to produce highly nano-porous and hydrated films, while increasing the DS concentration during polymerisation reduced porosity and increased densification of the polymer, generating a smoother polymer surface. However, herein we found polymer density to decrease with an increase in the XRU84 concentration in the polymerisation solution. The density of the polymer films calculated using QCM-D mass measurements of the polymerised films and profilometry thickness measurements was determined to be 3,106 kg/m^{-3} (0.2mg/ml^{-1} XRU84 loading), 1,306 kg/m^{-3} (2 mg/ml^{-1} XRU84 loading) and 1,136 kg/m^{-3} (20 mg/ml^{-1} XRU84 loading), respectively. The reduction in measured polymer density with increasing XRU84 loading is likely due to the highly hydrated properties of the large polyelectrolyte dopant XRU84, where an increase in the concentration of the anion in the polymerisation solution results in

an increase in its incorporation into the final polymer (through entrapment in the polymer matrix), reducing overall polymer density. We also note that the polymer density for the 0.2mg.ml^{-1} XRU loading presented a greater measured density measurement than theoretical density values previously reported the literature for PEDOT polymers (~1.06 kg.m^{-3})[50]. This is likely due to the highly hydrated nature of the XRU84 dopant and increased nano-porosity of the 0.2 mg.ml^{-1} XRU84 loaded films, increasing the overall hydration of the PEDOT-XRU84 film. This is supported by the increase in polymer hydrophilicity as XRU84 loading decreases (Table 1). Water coupled to the polymer cannot be excluded from the mass measurement using QCM-D technique, and therefore will increase the overall polymer mass, and thus increase the calculated density. Previous Raman and XPS characterisation of PPy polymerised with varying concentrations of the dopant DS showed no change in the oxidation state of the polymer with varying anion concentration, though the presence of the dopant within the polymer matrix was positively correlated with anion concentration during polymerisation[23, 49]. We propose a similar mechanism on increasing dopant entrapment, rather than polymer doping, with increasing XRU84 concentration in the polymerisation electrolyte, is likely to also be present in this system. Interestingly in this study as the XRU84 concentration in the polymerisation electrolyte was increased, the shear modulus of the polymer decreased significantly, which is contrary to what was seen in a recent study using DS to dope PPy[49]. The specific nature of the doping anion is known to considerably influence the modulus of electrochemically polymerised PEDOT[30, 32]. XRU84 is a large sulphated polysaccharide that while highly hydrophilic, can also form aggregates at higher concentrations via intermolecular hydrophobic interactions. This may result in aggregates presenting differing viscoelastic properties than those of individual XRU84 molecules, resulting in a change in the ultimate modulus of the polymerised film. Other studies using

similarly large biologically derived polyanions such as alginate to dope conducting polymers have also produced polymers with relatively lower moduli than those with synthetic or other smaller biomolecular dopants.[20] Further, the potential generated during the electrochemical polymerisation of films grown with an XRU84 electrolyte concentration of 20 mg/ml^{-1} at a constant current (0.25mA.cm^{-2}) was considerably larger (~1.4V) than those for the 0.2mg/ml^{-1} and 2 mg/ml^{-1} XRU84 concentrations (~1V) (data not shown). We propose this is likely the result of anion adsorption to the electrode surface, reducing the electrode active surface area while increasing anion incorporation into the polymer matrix.

Table 1. Summary of physical and interfacial properties of PEDOT polymer films

		PEDOT- XRU84		
		0.2mg/ml^{-1}	**2mg/ml^{-1}**	**20mg/ml^{-1}**
AFM	**RMS Roughness (nm)**	86 ± 4.6	27 ± 2.6	17.2 ± 1.6
	Increased Surface Area (%)	87.5 ± 10.4	28.4 ± 10.2	12.1 ± 3.5
QCM-D	**Mass (µg.cm^{-2})**	83.6 ± 2.2	55.8 ± 2.2	20.2 ± 4.8
	Shear Modulus (MPa)	3.17 ± 1.81	4.53 ± 1.81	0.29 ± 0.39
	Static Contact Angle (°)	17.5 ± 1.3	19.0 ± 3.1	30.0 ± 0.9
	Thickness (nm)	385 ± 47	397 ± 67	123 ± 14

B. Electrochemical Characterisation

Cyclic voltammetry of an unmodified gold electrode in PBS mainly passed current through capacitance (Figure 2). A very small oxidation peak at 270 mV is associated with oxide

formation and a reduction current below -250 mV is due to oxide and residual oxygen reduction[51]. After modifying the electrode with PEDOT-XRU84, the cyclic voltammetry became featureless over the potential window of 0.8 to -0.8 V. This indicates the gold surface oxide formation and reduction processes, and oxygen reduction is prevented or significantly reduced in relative magnitude to the redox response of the conducting polymer after surface modification.

The charge passed during the cathodic and anodic sweeps was calculated by integrating the current-time plot then divided by the nominal electrode area, providing a charge storage capacity (CSC). The CSC is related to the charge injection capacity obtained from chronopotentiometric pulsing[52]. A larger CSC allows an electrode to inject current into tissue via safe charge transfer mechanisms rather than through water electrolysis. An increase in CSC can be achieved by increasing an electrodes capacitance. The CSC of PEDOT-XRU84 0.2 mg/ml^{-1} bioloaded film was significantly larger than the bare gold, but decreased with increasing XRU concentration (Table 2). Assuming surface capacitance is unaffected by polymer loading, this is consistent with PEDOT-XRU84 0.2 mg/ml^{-1} bioloaded films having the highest surface roughness, enabling greater capacitance charge.

Charge transfer across the electrode-tissue interface may not be fully reversible. The ratio of CSC_c to CSC_a provides an indication of the reversibility of any redox processes and the stability of the electrode to current passage[53]. The CSC_c of the unmodified gold electrode is significantly greater than the CSC_a, indicating the electrode would be unstable over multiple current pulses[52]. In contrast, the ratio of CSC_c to CSC_a on the PEDOT-XRU84 electrodes is close to 1, which should result in a more stable electrode when it is used for electrical stimulation of tissue.

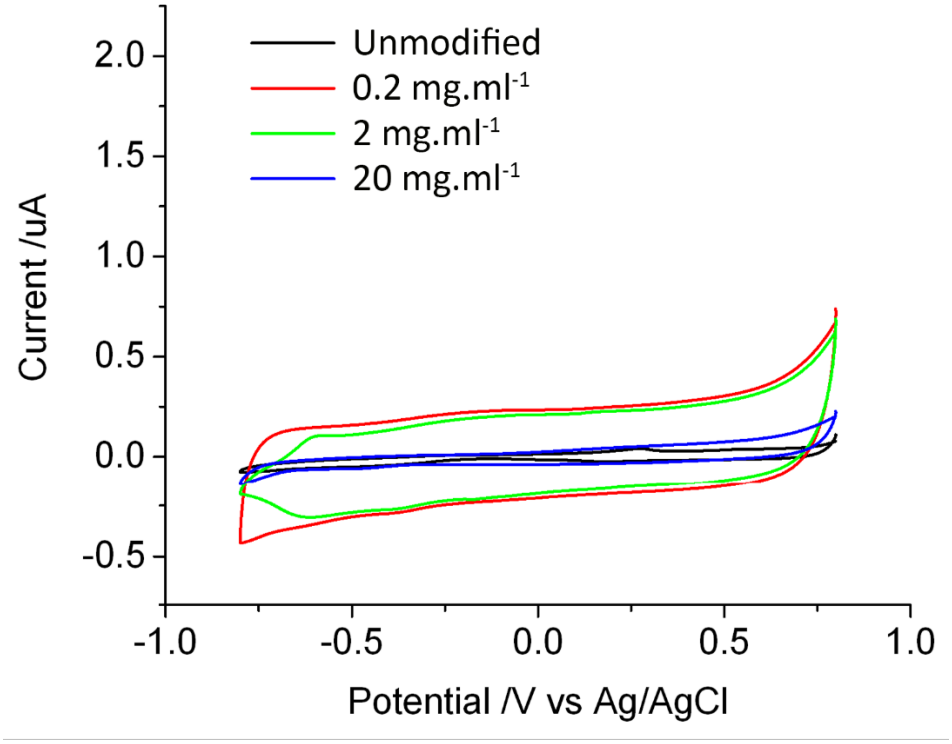

FIG 2. Cyclic voltammetry of unmodified gold and PEDOT- XRU84 at increasing electrolyte concentration.

The impedance of the electrode is measured to assess the thermal noise and signal-to-noise ratio for electrical recordings of tissue. Gold and PEDOT- XRU84 modified electrodes in PBS displayed an increasing impedance with decreasing frequency (Figure 3). The phase angle indicated the electrodes behaved as a resistor at high frequencies and a capacitor at low frequencies. The impedance at low frequencies can predict an electrodes electrophysiological performance[54]. The impedance at 10 Hz was significantly reduced by modifying the gold with PEDOT- XRU84 grown at the lowest XRU84 electrolyte concentration (0.2 mg/ml^{-1}) and then increased at higher XRU84 concentrations.

The impedance of the electrodes could be modelled with an equivalent circuit. The unmodified gold and PEDOT- XRU84 films grown with 0.2 and 2 mg/ml^{-1} XRU84 electrolyte concentrations could be fit with a series solution resistance (R1) and constant phase element (CPE1) to account for the electrical double layer. The use of a constant phase element rather than a capacitor is thought to be due to inhomogeneous current distribution over the electrode surface or surface roughness. At 20 mg/ml^{-1} bioloaded PEDOT- XRU84 films, a polarisation resistance (R2) needed to be added in parallel with the constant phase element. The solution resistance was unaffected by the surface modification (Table 2). The admittance (Q_0) associated with the constant phase element was far greater after surface modification, but decreased with increasing XRU84 concentration. The correlation of Q_0 with RMS roughness suggests current inhomogeneity is at least partly due to surface roughness. This again indicates PEDOT grown with 0.2mg/ml^{-1} XRU84 has the highest capacitance of the electrodes tested. The large increase in impedance with 20 mg/ml^{-1} bioloaded PEDOT-XRU84 and the addition of a polarisation resistance may also be due to adsorption of dopant on the surface of the polymer, reducing the electrodes effective area.

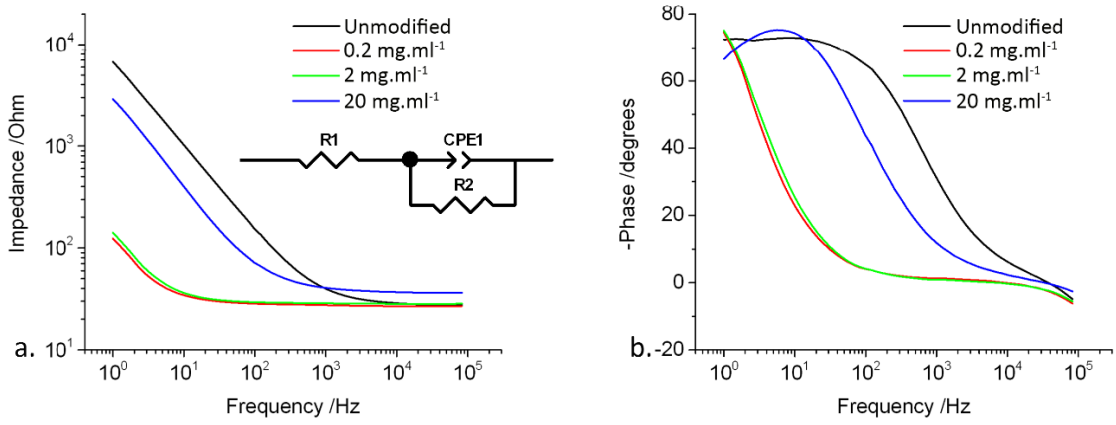

FIG 3. EIS of unmodified gold and PEDOT- XRU84 at increasing electrolyte concentration. Equivalent circuit fitting of unmodified and PEDOT- XRU84 at 0.2 mg/ml^{-1} and 2 mg/ml^{-1} included R1 and CPE1, fitting of PEDOT- XRU84 20 mg/ml^{-1} required addition of R2.

Table 2. Summary of electrochemical properties of PEDOT polymer films

			PEDOT- XRU84		
		Unmodified	**0.2 mg/ml^{-1}**	**2 mg/ml^{-1}**	**20 mg/ml^{-1}**
Voltammetry	**CSC_c (mC cm^{-2})**	68.9 ± 0.8	434 ± 25.6	365 ± 26.2	98.1 ± 10.3
	CSC_a (mC cm^{-2})	37.5 ± 0.6	479 ± 25.9	396 ± 39.3	87.0 ± 8.8
EIS	**Impedance 10 Hz (Ohm)**	885 ± 197	33.9 ± 0.8	39.4 ± 4.5	414 ± 19.5
	Solution Resistance (Ohm)	28 ± 1	27 ± 1	31 ± 3	32 ± 7
	Q_0 / 10^{-6} (S s$^{1/2}$)	38 ± 8	1580 ± 56	1310 ± 112	67 ± 1
	n	0.83 ± 0.00	0.91 ± 0.01	0.90 ± 0.01	0.87 ± 0.01
	Polarisation Resistance (kOhm)	-	-	-	13.2 ± 5.0

C. QCM-D Characterisation of Protein Adsorption to PEDOT-XRU84 Films

QCM-D was used to study the interaction of the proteins fibrinogen, transferrin and collagen to the PEDOT-XRU84 polymer materials. All three proteins play a crucial role in various stages of the wound healing process. Fibrinogen is critical for blood clotting, mediating cellular and matrix interactions, and inflammation[55], while collagen is critical in maintaining the structural integrity of the extracellular matrix, where constant remodelling drives cell behaviour and tissue function[56]. Transferrin is vital for the transport of iron around the body, with surface adsorbed transferrin shown to play a role in angiogenesis[28]. The raw frequency and dissipation curves detailing the protein interactions with the polymers are illustrated in Figure 4. Typical negative frequency shifts are exhibited for the proteins for all three PEDOT- XRU84 variants, with a negative Δf generated as protein is introduced into the QCM-D measurement chamber and adsorbs to the polymer surface, with protein adsorption continuing until fresh PBS without protein is introduced into the chamber after 60 mins, where the Δf plateaus. For collagen, a negative frequency shift was coupled with a positive ΔD for all PEDOT- XRU84 films, indicating the adsorption of a viscoelastic layer to the polymer surface. This was not the case for fibrinogen and transferrin adsorption to PEDOT films polymerised with the lowest XRU84 concentration (0.2 mg/ml^{-1}), where rather than a positive ΔD, a negative ΔD was observed during protein adsorption (Figure 4 a,c).

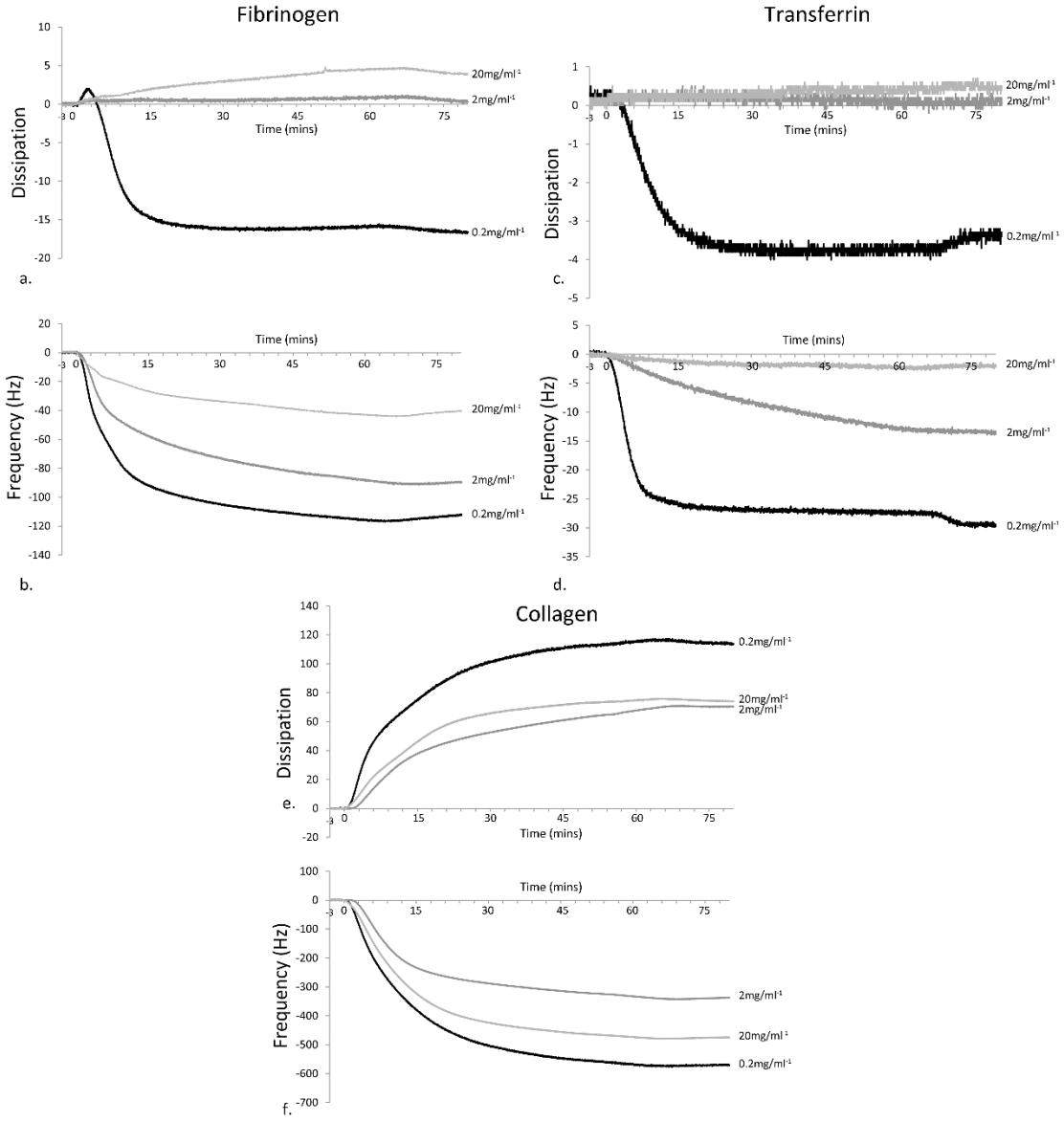

FIG 4. Representative raw frequency and dissipation parameter shifts in response to the adsorption of Fb (a,b), TF (c,d) and CG (e,f) to PEDOT- XRU84 films as a function of the XRU84 loading during polymerisation.

The QCM-D raw data was modelled in order to quantify the areal mass adsorbed to each polymer, with the adsorbed mass normalised as a function of the polymer surface area, measured using AFM, enabling a direct comparison between each of the PEDOT- XRU84 polymer films. All protein adsorption data were quantified using the Voigt viscoelastic

model, however it should be noted that the application of the Voigt model to the data sets presenting negative dissipation shifts (collagen and transferrin adsorption to XRU84 loading concentrations of 0.2mg.ml^{-1}) was highly problematic, due to the inability for the model to consider negative dissipation values. With modelling of these two data sets presenting similar mass values when tested with both the Voigt and Sauerbrey models, we have chosen to present the Voigt modelled results herein for consistency (noted with * in Figure 5). We have additionally included the mean frequency and dissipation values for all experiments in the supplemental material (S1).

There was no significant difference in the fibrinogen adsorption to the three PEDOT- XRU84 films, with adsorption of 1007 ± 87, 1179 ± 239 and 843 ± 138 ng.cm^2 adsorbed to the 0.2 mg/ml^{-1}, 2 mg/ml^{-1}, and 20 mg/ml^{-1} XRU84 bioloaded films, respectively (Figure 5). Figure 6 (a) illustrates representative Δ*D*/Δ*f* plots of fibrinogen adsorption to the variable PEDOT-XRU84 films, with the final Δ*D*/Δ*f* ratio presented in Figure 5d. The Δ*D*/Δ*f* plot reveals information relating to the adsorption profile and the viscoelastic properties of the surface bound protein layer during the adsorption process[57]. The final Δ*D*/Δ*f* ratio describes the final viscoelastic nature of the adsorbed protein layer, with an increase in the Δ*D*/Δ*f* illustrative of a more viscoelastic, hydrated adsorbed mass[58-60]. The Δ*D*/Δ*f* plot for fibrinogen adsorption to the PEDOT polymer films reveals the dynamic process of protein adsorption to differ considerably as a function of variable XRU84 loading during polymerisation (Figure 6a). Fibrinogen adsorption to the 20mg/ml^{-1} bioloaded films reproducibly demonstrated two separate phases during protein adsorption, with an initial rapid phase on protein introduction into the QCM-D chamber, followed by a slower secondary phase that also produced a more viscoelastic adsorbed layer than the initial layer. Fibrinogen adsorption to the 2 mg/ml^{-1} bioloaded PEDOT- XRU84 films provided a consistent

shift that did not deviate in gradient, revealing all protein adsorption to occur in a single phase or mode. Fibrinogen adsorption to the lowest XRU84 polymer loading however presented a far more dynamic and complex adsorption process. After an initial phase that saw an increase in dissipation with protein adsorption (-ve Δ*f*) to the polymer surface, a clear transition is reached at ~ -25 Hz where the Δ*D* begins to decrease, followed by a third phase that results in the Δ*D* reaching negative values. The final Δ*D*/Δ*f* reveals significant differences in the viscoelastic properties of the adsorbed layers, with the most rigid, elastic adlayer presented on the 0.2 mg/ml^{-1} bioloaded PEDOT- XRU84 films (Δ*D*/Δ*f* ratio of -0.12 ± 0.06), with fibrinogen layers on the 2 mg/ml^{-1} and 20 mg/ml^{-1} bioloaded polymers becoming increasingly more hydrated and viscoelastic (Δ*D*/Δ*f* ratio of 0.019 ± 0.023 and 0.131 ± 0.040 for 2 and 20 mg/ml^{-1} bioloading, respectively) (Figure 6d).

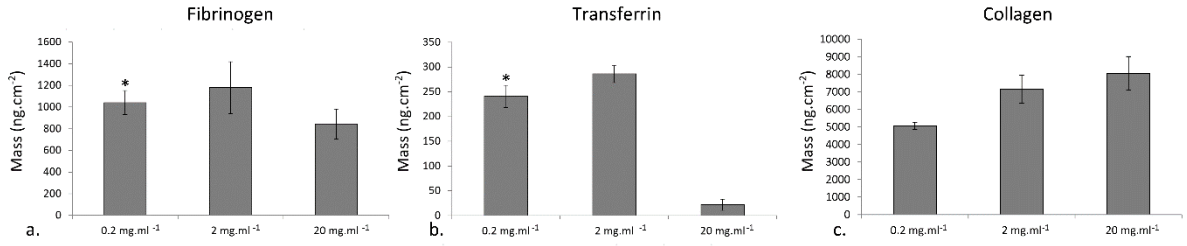

FIG 5. QCM-D modelled mass values (ng.cm^{-2}) for the adsorption of Fb (a), TF (b) and CG (c) to PEDOT /polymerised in the presence of either 0.2, 2 or 20 mg.ml^{-1} of XRU84. Error bars represent 95% confidence intervals around the mean. * indicates data presenting negative dissipation values.

Fibrinogen plays several vital roles in wound healing processes, including in forming blood clots after injury, interactions with extracellular matrix components and cells that can drive cell responses such as proliferation, migration and adhesion, as well as modulating the transition from wound inflammation to tissue repair (for review, see Laurens et. al.[61]). Previous studies have shown fibrinogen to exhibit multi-phase adsorption processes to

surfaces, with Roach et al.[62] describing a two phase adsorption process for fibrinogen to OH and CH_3 modified surfaces. Therein an initial fast adsorption process was proposed to correlate to the binding of the fibrinogen dimer with the backbone parallel to the surface, followed by re-orientation of the protein perpendicular to the surface, providing further space for additional protein from solution to bind. The authors proposed this behaviour to be driven by hydrophobic interactions between the protein molecules.

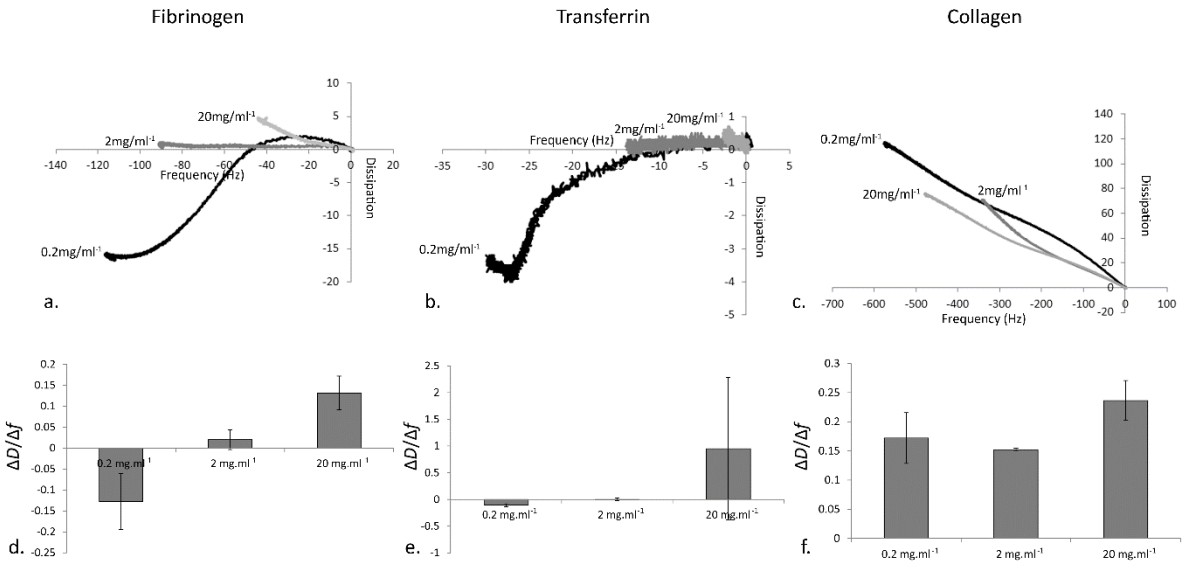

FIG 6. Δ*D*/Δ*f* plots for the adsorption of fibrinogen (a), tranferrin (b) and collagen (c) to PEDOT polymerised in the presence of 0.2, 2 or 20mg/ml^{-1} XRU84. Final Δ*D*/Δ*f* ratio's for fibrinogen (c), transferrin (d) and collagen (e) adsorption to the variable PEDOT- XRU84 materials are also presented. All error bars represent 95% confidence intervals around the mean.

The theoretical mass adsorption of fibrinogen in the side on or end on configuration is 420 and 3000 ng.cm^2 for QCM measurements, respectively, accounting for the technique

sensitivity to hydrodynamically coupled water[63]. For all films the mass adsorption was between 843 and 1179 ng.cm^{-2}, indicating a heterogeneous population of protein orientation on the surface. The substantial negative Δ*D* presented on the 0.2mg/ml^{-1} bioloaded polymer film is difficult to explain without considering the influence of the fibrinogen adsorption on the interfacial environment of the polymer film. Negative dissipation shifts may be derived from a number of mechanisms, such as the crosslinking of a polymer that results in an increase in polymer rigidity, and changes in the viscoelastic properties of the bulk material through other mechanisms, such as dehydration. We propose the adsorption of the fibrinogen onto the 0.2 mg/ml^{-1} bioloaded PEDOT- XRU84 films is influenced by the interfacial surface topography and highly hydrated nature of the polymer film, altering the interfacial hydration of the polymer. Surface roughness has previously been proposed to be a factor that can drive fibrinogen re-orientation on a surface[60]. From the QCM-D Δ*f*/Δ*D* plot, it is clear that a number of dynamic processes are occurring during the initial minutes of adsorption of fibrinogen to the 0.2mg/ml^{-1} polymer. We propose that the dramatic shift in dissipation could be due to the re-orientation of the fibrinogen molecules during adsorption, likely driven by a combination of interfacial surface roughness and polymer chemistry, generating a more hydrophobic interface at the polymer surface. Given the rough surface morphology of the film, the change in the surface energy at the polymer interfacial environment has the effect of dehydrating interstitial pores and spaces, causing an increase in rigidity and thus a decrease in bulk dissipation. This is supported through contact angle measurements taken of the PEDOT- XRU84 0.2 mg/ml^{-1} bioloaded film before and after fibrinogen adsorption, with the contact angle increasing from 22 ± 1.2° before fibrinogen adsorption to 76 ± 0.6° after fibrinogen adsorption (data not shown). Therefore, the negative dissipation shift recorded here is likely attributed to a

combination of the removal of interfacial water at the polymer surface, in addition to the properties of the fibrinogen protein layer.

Transferrin adsorption was significantly reduced on PEDOT- XRU84 films polymerised with the highest XRU84 concentration (20 mg/ml^{-1}), relative to the 0.2 mg/ml^{-1} and 2 mg/ml^{-1} bioloaded polymer films (Figure 5b). Transferrin is an iron binding glycoprotein that plays a vital role in iron transport within the circulatory system[64]. Transferrin protein controls the delivery of iron at the wound site, with iron playing a critical role in skin and cutaneous wound healing processes[65]. Furthermore, surface adsorbed transferrin has been shown to be a major angiogenic molecule, facilitating the migration of endothelial cells[28], and therefore transferrin binding to the PEDOT-XRU84 material may promote cell migration and tissue regeneration. There was no significant difference in the final $\Delta D/\Delta f$ ratio for transferrin adsorption to the PEDOT-XRU84 films, although the standard deviation in measurements for the 20 mg/ml^{-1} bioloaded film were quite large (Figure 6e). The general trends of the final $\Delta D/\Delta f$ were similar to that seen for fibrinogen, with the ratio increasing with increasing XRU84 concentration in the polymerisation solution, with this also reflected in the $\Delta D/\Delta f$ plot, where the transferrin adsorption profile closely resembled the processes seen for fibrinogen. Transferrin adsorption to the 2 and 20 mg/ml^{-1} bioloaded films demonstrated relatively small positive frequency shifts that exhibited single or dual phase adsorption profiles, while transferrin adsorption to the 0.2 mg/ml^{-1} bioloaded film resulted in a significantly larger negative ΔD as protein adsorbed to the polymer surface. We propose transferrin adsorption to the 0.2 mg/ml^{-1} bioloaded PEDOT- XRU84 films to likely follow a similar mechanism to that described for fibrinogen adsorption, where the protein orientation and organisation on the rougher and more nano-porous 0.2 mg/ml^{-1} XRU84 films presents a more hydrophobic interface, resulting in dehydration of the polymer interface.

Collagen is the major element of ECM networks, as a major component of highly structured 3D scaffolds that promote cell attachment, proliferation and differentiation processes[66-67]. These properties have seen collagen widely used in the production of biomaterials to promote wound healing and tissue regeneration and repair (for review, see Chattopadhyay and Raines[67]). PEDOT films with the higher XRU84 loading (2 and 20 mg/ml^{-1}) provided significantly greater overall adsorption of collagen compared to the lowest XRU84 loading (Figure 5C). All collagen layers presented similar viscoelastic properties, with all films demonstrating a highly viscoelastic protein layer, with the highest mean $\Delta D/\Delta f$ ratio demonstrated for the 20 mg/ml^{-1} XRU84 bioloaded films.

D. Human Dermal Fibroblast Cell Viability and Morphology on PEDOT-XRU84 Composite Polymers

Human dermal fibroblasts were used to determine the biocompatibility of the different PEDOT-XRU84 composite materials, and their potential for use in wound healing applications. All three PEDOT-XRU84 composite films showed excellent cell viability after 2 hrs, with all films illustrating a cell viability level of > 96% (Figure 7, Supplemental Figure 2). The cell viability for all samples decreased after 24 hrs of culture, although remained high, with cell viability values of 83 ± 12% (0.2 mg/ml^{-1}), 88 ± 17% (2 mg/ml^{-1}), and 73 ± 25% (20mg/ml^{-1}) for the respective XRU84 bioloaded films. There were no significant differences evident for cell viability between the PEDOT-XRU84 films for either 2 hr or 24 hr incubation times.

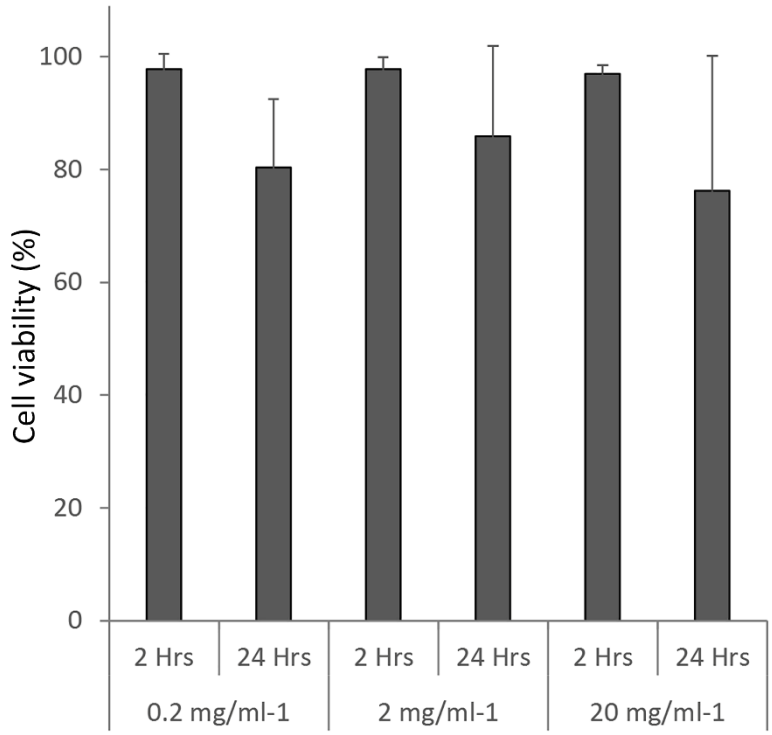

FIG 7. Viability of Human dermal fibroblasts seeded on PEDOT-XRU84 polymerised with 0.2 mg/ml^{-1}, 2 mg/ml^{-1} or 20 mg/ml^{-1} XRU84 electrolyte concentration after 2h and 24h of culture. Data showed no significant difference ($p \geq 0.05$) between samples from same time point.

Cell morphology was visualised via staining of the actin filaments and nuclei of cells adhered to the PEDOT-XRU84 films (Figure 8). After 2 hrs of culture, a variety of cell cytoskeletal morphologies are evident on all three films, indicative of cells at different stages of cell adhesion and spreading on the polymer surfaces. After 24 hrs, cells demonstrated a more homogenous morphology, with actin bundles extending across the cell body, illustrating excellent cell spreading. All three polymer surfaces showed similar levels of cells spreading and attachment, demonstrating their ability to interface effectively with human dermal fibroblasts.

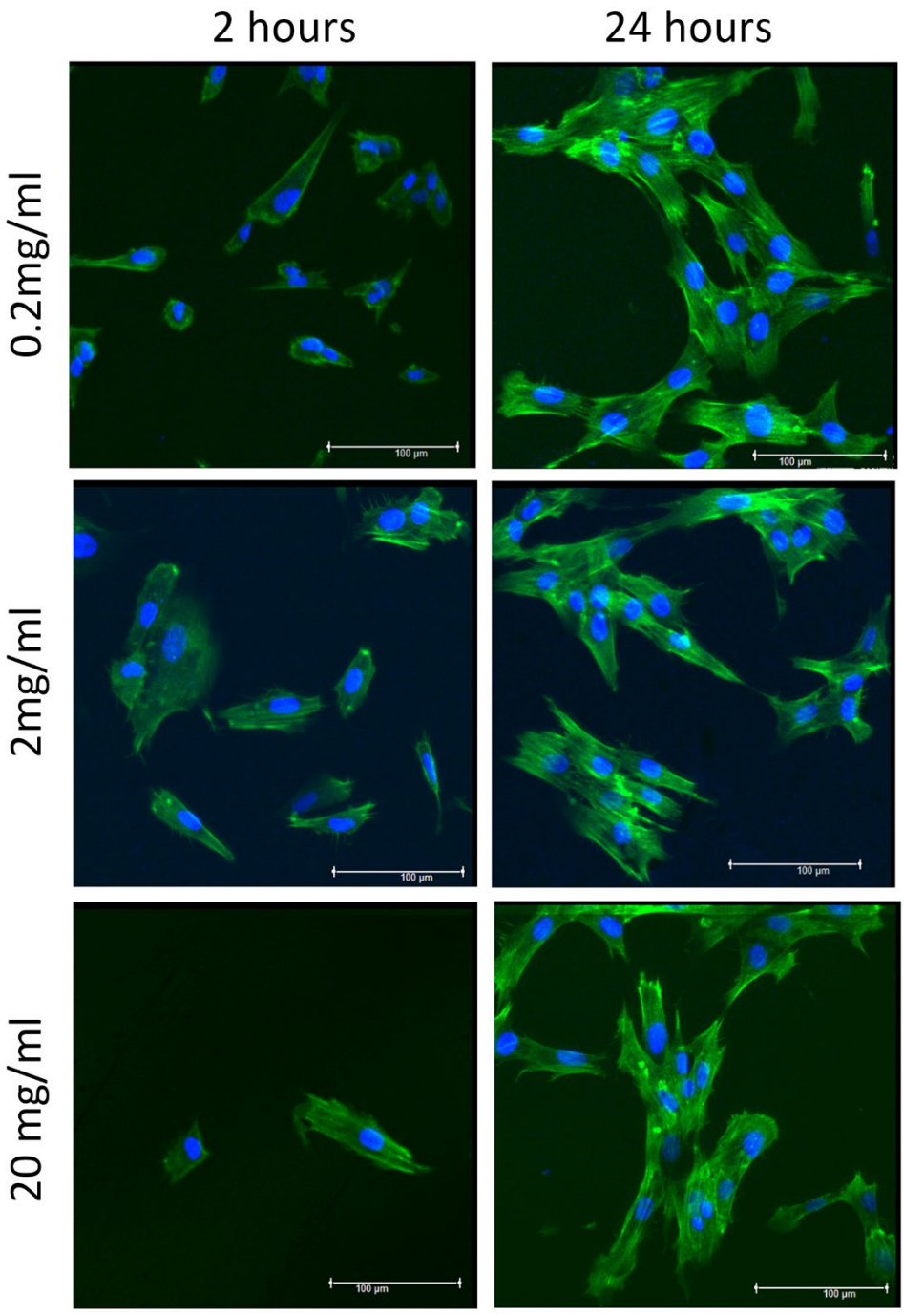

FIG 8. Fluorescent images of Human Dermal Fibroblast cytoskeleton visualised with phalloidin staining demonstrating changes in cell attachment on PEDOT-XRU84 (0.2 $mg.ml^{-1}$, 2 $mg.ml^{-1}$ and 20 $mg.ml^{-1}$ XRU84 bioloading) polymer samples after 2h and 24h of culture. Actin filaments are stained green and cell nuclei are stained in blue.

IV. Summary and Conclusions

Materials used in dressings and bandages for wound healing applications have traditionally focused on the prevention of infection, and maintaining a moist wound environment while removing excess moisture discharged during the healing process. Recent advances in the area of materials science has focused on improving on these traditional approaches by developing materials that will also directly interface with the wound site and support electrostimulation promoting staged wound healing processes towards the generation of functional, rather than fibrotic tissue. Herein we present the conducting polymer biomaterial PEDOT doped with a rhamnose rich and large molecular weight (>600kDa) xylorhamnouronic glycan (XRU84) as a new biomaterial for wound healing applications. We characterised polymer interfacial, mechanical and electrical properties that proved suitable for interfacing with biological systems. Furthermore, we studied the adsorption and interfacing of proteins known to play a critical role during the wound healing process. The adsorption mass of collagen increased with greater XRU84 bioloading, while that of transferrin decreased dramatically on the 20 mg/ml^{-1} bioloaded films. The mechanical properties, or conformational properties, of the adsorbed proteins were also considerably altered as a function of XRU84 electrolyte concentration, with both fibrinogen and transferrin demonstrating more rigid, dehydrated proteinaceous layers on the films incorporating lower amounts of XRU84, while no such difference was evident for collagen. Preliminary cell studies demonstrated the PEDOT-XRU84 polymer films to present excellent cell viability and cell spreading after 24hrs, highlighting their ability to interface effectively with the PEDOT-XRU84 biomaterials. Future work should focus on how the variable modes of protein binding observed here interact with processes critical to wound healing. Studies of cell adhesion and migration, as well as the impact of electrical stimulation on cells using

the biocomposite polymers will also provide further avenues for investigation for application of the materials for accelerated healing processes and extra-cellular matrix development.

Acknowledgements

The authors gratefully acknowledge funding from the Australian Research Council (ARC) through the Australian Centre of Excellence for Electromaterials Science (CE140100012). We also thank the Australian National Fabrication Facility for access to equipment.

References

1. Gurtner, G. C.; Werner, S.; Barrandon, Y.; Longaker, M. T., Wound repair and regeneration. *Nature* **2008,** *453* (7193), 314-321.
2. Talikowska, M.; Fu, X.; Lisak, G., Application of conducting polymers to wound care and skin tissue engineering: A review. *Biosensors Bioelectron.* **2019,** *135*, 50-63.
3. Martin, P., Wound healing--aiming for perfect skin regeneration. *Science* **1997,** *276* (5309), 75-81.
4. Das, S.; Baker, A. B., Biomaterials and Nanotherapeutics for enhancing Skin wound Healing. *Frontiers in Bioengineering and Biotechnology* **2016,** *4*.
5. Aarabi, S.; Longaker, M. T.; Gurtner, G. C., Hypertrophic scar formation following burns and trauma: new approaches to treatment. *PLoS Med.* **2007,** *4* (9), e234.
6. Dhivya, S.; Padma, V. V.; Santhini, E., Wound dressings - a review. *Biomedicine* **2015,** *5* (4), 22-22.
7. Boateng, J. S.; Matthews, K. H.; Stevens, H. N. E.; Eccleston, G. M., Wound Healing Dressings and Drug Delivery Systems: A Review. *J. Pharm. Sci.* **2008,** *97* (8), 2892-2923.
8. Hutchinson, J. J.; McGuckin, M., Occlusive dressings: A microbiologic and clinical review. *Am. J. Infect. Control* **1990,** *18* (4), 257-268.
9. KANNON, G. A.; GARRETT, A. B., Moist Wound Healing with Occlusive Dressings. *Dermatol. Surg.* **1995,** *21* (7), 583-590.
10. Baum, T. M.; Busuito, M. J., Use of a glycerin-based gel sheeting in scar management. *Advances in wound care : the journal for prevention and healing* **1998,** *11* (1), 40-43.
11. Gu, Q.; Wang, S.; Wang, Q.; Wei, X., [Application status and research progess of alginate dressings]. *Zhongguo xiu fu chong jian wai ke za zhi = Zhongguo xiufu chongjian waike zazhi = Chinese journal of reparative and reconstructive surgery* **2014,** *28* (2), 255-258.
12. Mian, M.; Beghe, F.; Mian, E., Collagen as a pharmacological approach in wound healing. *Int. J. Tissue React.* **1992,** *14 Suppl*, 1-9.
13. Prosdocimi, M.; Bevilacqua, C., Exogenous hyaluronic acid and wound healing: an updated vision. *Panminerva Med.* **2012,** *54* (2), 129-35.
14. Ruszczak, Z., Effect of collagen matrices on dermal wound healing. *Adv. Drug Delivery. Rev.* **2003,** *55* (12), 1595-1611.
15. Farahani, R. M.; Kloth, L. C., The hypothesis of 'biophysical matrix contraction': wound contraction revisited. *Int. Wound J.* **2008,** *5* (3), 477-82.

16. Ud-Din, S.; Bayat, A., Electrical Stimulation and Cutaneous Wound Healing: A Review of Clinical Evidence. *Healthcare (Basel)* **2014,** *2* (4), 445-467.
17. Boateng, J.; Catanzano, O., Advanced Therapeutic Dressings for Effective Wound Healing--A Review. *J. Pharm. Sci.* **2015,** *104* (11), 3653-80.
18. Wallace, G.; Spinks, G., Conducting polymers–bridging the bionic interface. *Soft Matter* **2007,** *3* (6), 665-671.
19. Stewart, E.; Kobayashi, N. R.; Higgins, M. J.; Quigley, A. F.; Jamali, S.; Moulton, S. E.; Kapsa, R. M.; Wallace, G. G.; Crook, J. M., Electrical stimulation using conductive polymer polypyrrole promotes differentiation of human neural stem cells: a biocompatible platform for translational neural tissue engineering. *Tissue Engineering Part C: Methods* **2014,** *21* (4), 385-393.
20. Molino, P. J.; Yue, Z.; Zhang, B.; Tibbens, A.; Liu, X.; Kapsa, R. M. I.; Higgins, M. J.; Wallace, G. G., Influence of Biodopants on PEDOT Biomaterial Polymers: Using QCM-D to Characterize Polymer Interactions with Proteins and Living Cells. *Advanced Materials Interfaces* **2014,** *1* (3), n/a-n/a.
21. Svennersten, K.; Berggren, M.; Richter-Dahlfors, A.; Jager, E. W. H., Mechanical stimulation of epithelial cells using polypyrrole microactuators. *Lab on a Chip* **2011,** *11* (19), 3287-3293.
22. Thompson, B. C.; Richardson, R. T.; Moulton, S. E.; Evans, A. J.; O'Leary, S.; Clark, G. M.; Wallace, G. G., Conducting polymers, dual neurotrophins and pulsed electrical stimulation - Dramatic effects on neurite outgrowth. *J. Control. Release* **2010,** *141* (2), 161-167.
23. Molino, P. J.; Higgins, M. J.; Innis, P. C.; Kapsa, R. M. I.; Wallace, G. G., Fibronectin and Bovine Serum Albumin Adsorption and Conformational Dynamics on Inherently Conducting Polymers: A QCM-D Study. *Langmuir* **2012,** *28* (22), 8433-8445.
24. Wan, A. M. D.; Brooks, D. J.; Gumus, A.; Fischbach, C.; Malliaras, G. G., Electrical control of cell density gradients on a conducting polymer surface. *Chem. Commun.* **2009,** (35), 5278.
25. Gumus, A.; Califano, J. P.; Wan, A. M. D.; Huynh, J.; Reinhart-King, C. A.; Malliaras, G. G., Control of cell migration using a conducting polymer device. *Soft Matter* **2010,** *6* (20), 5138-5142.
26. CLARK, R. A. F., Fibrin and Wound Healing. *Ann. N. Y. Acad. Sci.* **2001,** *936* (1), 355-367.
27. Brett, D., A Review of Collagen and Collagen-based Wound Dressings. *Wounds : a compendium of clinical research and practice* **2008,** *20* (12), 347-56.
28. Carlevaro, M. F.; Albini, A.; Ribatti, D.; Gentili, C.; Benelli, R.; Cermelli, S.; Cancedda, R.; Cancedda, F. D., Transferrin Promotes Endothelial Cell Migration and Invasion: Implication in Cartilage Neovascularization. *The Journal of Cell Biology* **1997,** *136* (6), 1375.
29. Gelmi, A.; Higgins, M. J.; Wallace, G. G., Resolving Sub-Molecular Binding and Electrical Switching Mechanisms of Single Proteins at Electroactive Conducting Polymers. *Small* **2013,** *9* (3), 393-401.
30. Molino, P. J.; Yue, Z.; Zhang, B.; Tibbens, A.; Liu, X.; Kapsa, R. M. I.; Higgins, M. J.; Wallace, G. G., Influence of Biodopants on PEDOT Biomaterial Polymers: Using QCM-D to Characterize Polymer Interactions with Proteins and Living Cells. *Advanced Materials Interfaces* **2014,** *1* (3), 1300122-n/a.
31. Molino, P. J.; Tibbens, A.; Kapsa, R. M. I.; Wallace, G. G., Incorporating Biodopants into PEDOT Conducting Polymers: Impact of Biodopant on polymer properties and biocompatibility. *MRS Proceedings* **2013,** *1569*, 225-230.
32. Molino, P. J.; Garcia, L.; Stewart, E. M.; Lamaze, M.; Zhang, B.; Harris, A. R.; Winberg, P.; Wallace, G. G., PEDOT doped with algal, mammalian and synthetic dopants: polymer properties, protein and cell interactions, and influence of electrical stimulation on neuronal cell differentiation. *Biomater Sci* **2018,** *6* (5), 1250-1261.
33. Green, R. A.; Lovell, N. H.; Poole-Warren, L. A., Impact of co-incorporating laminin peptide dopants and neurotrophic growth factors on conducting polymer properties. *Acta Biomater.* **2010,** *6* (1), 63-71.
34. Gilmore, K. J.; Kita, M.; Han, Y.; Gelmi, A.; Higgins, M. J.; Moulton, S. E.; Clark, G. M.; Kapsa, R.; Wallace, G. G., Skeletal muscle cell proliferation and differentiation on polypyrrole substrates doped with extracellular matrix components. *Biomaterials* **2009,** *30* (29), 5292-304.

35. Zhang, B.; Molino, P. J.; Harris, A. R.; Yue, Z.; Moulton, S. E.; Wallace, G. G., Conductive and protein resistant polypyrrole films for dexamethasone delivery. *Journal of Materials Chemistry B* **2016,** *4* (15), 2570-2577.
36. Muller, R.; Yue, Z.; Ahmadi, S.; Ng, W.; Grosse, W. M.; Cook, M. J.; Wallace, G. G.; Moulton, S. E., Development and validation of a seizure initiated drug delivery system for the treatment of epilepsy. *Sensors Actuators B: Chem.* **2016,** *236*, 732-740.
37. Meng, S.; Rouabhia, M.; Shi, G.; Zhang, Z., Heparin dopant increases the electrical stability, cell adhesion, and growth of conducting polypyrrole/poly (L, L-lactide) composites. *Journal of Biomedical Materials Research Part A* **2008,** *87* (2), 332-344.
38. Collier, J. H.; Camp, J. P.; Hudson, T. W.; Schmidt, C. E., Synthesis and characterization of polypyrrole–hyaluronic acid composite biomaterials for tissue engineering applications. *J. Biomed. Mater. Res.* **2000,** *50* (4), 574-584.
39. Rouabhia, M.; Park, H.; Meng, S.; Derbali, H.; Zhang, Z., Electrical Stimulation Promotes Wound Healing by Enhancing Dermal Fibroblast Activity and Promoting Myofibroblast Transdifferentiation. *PLoS One* **2013,** *8* (8), e71660.
40. Wang, Y.; Rouabhia, M.; Lavertu, D.; Zhang, Z., Pulsed electrical stimulation modulates fibroblasts' behaviour through the Smad signalling pathway. *J. Tissue Eng. Regen. Med.* **2015**.
41. Wan, A. M.-D.; Inal, S.; Williams, T.; Wang, K.; Leleux, P.; Estevez, L.; Giannelis, E. P.; Fischbach, C.; Malliaras, G. G.; Gourdon, D., 3D conducting polymer platforms for electrical control of protein conformation and cellular functions. *Journal of Materials Chemistry B* **2015,** *3* (25), 5040-5048.
42. Lahaye, M.; Robic, A., Structure and functional properties of ulvan, a polysaccharide from green seaweeds. *Biomacromolecules* **2007,** *8* (6), 1765-1774.
43. Chiellini, F.; Morelli, A., Ulvan: A versatile platform of biomaterials from renewable resources. *Biomaterials—Physics and Chemistry* **2011**, 75-98.
44. Mao, W.; Zang, X.; Li, Y.; Zhang, H., Sulfated polysaccharides from marine green algae Ulva conglobata and their anticoagulant activity. *J. Appl. Phycol.* **2006,** *18* (1), 9-14.
45. Gadenne, V.; Lebrun, L.; Jouenne, T.; Thebault, P., Antiadhesive activity of ulvan polysaccharides covalently immobilized onto titanium surface. *Colloids Surf. B. Biointerfaces* **2013,** *112*, 229-236.
46. Chen, X.; Yue, Z.; Winberg, P. C.; Dinoro, J. N.; Hayes, P.; Beirne, S.; Wallace, G. G., Development of rhamnose-rich hydrogels based on sulfated xylorhamno-uronic acid toward wound healing applications. *Biomaterials Science* **2019**.
47. Kang, L.; Liu, X.; Yue, Z.; Chen, Z.; Baker, C.; Winberg, C. P.; Wallace, G. G., Fabrication and In Vitro Characterization of Electrochemically Compacted Collagen/Sulfated Xylorhamnoglycuronan Matrix for Wound Healing Applications. *Polymers* **2018,** *10* (4).
48. Molino, P. J.; Tibbens, A.; Kapsa, R. M. I.; Wallace, G. G., Incorporating Biodopants into PEDOT Conducting Polymers: Impact of Biodopant on polymer properties and biocompatibility. *MRS Online Proceedings Library* **2013,** *1569*, 225-230.
49. Molino, P. J.; Innis, P. C.; Higgins, M. J.; Kapsa, R. M. I.; Wallace, G. G., Influence of biopolymer loading on the physiochemical and electrochemical properties of inherently conducting polymer biomaterials. *Synth. Met.* **2015,** *200*, 40-47.
50. Lenz, A.; Kariis, H.; Pohl, A.; Persson, P.; Ojamäe, L., The electronic structure and reflectivity of PEDOT:PSS from density functional theory. *Chem. Phys.* **2011,** *384* (1), 44-51.
51. Xu, X.; Makaraviciute, A.; Pettersson, J.; Zhang, S.-L.; Nyholm, L.; Zhang, Z., Revisiting the factors influencing gold electrodes prepared using cyclic voltammetry. *Sensors Actuators B: Chem.* **2019,** *283*, 146-153.
52. Harris, A. R.; Newbold, C.; Carter, P.; Cowan, R.; Wallace, G. G., Using Chronopotentiometry to Better Characterize the Charge Injection Mechanisms of Platinum Electrodes Used in Bionic Devices. *Front. Neurosci.* **2019,** *13* (380).

53. Harris, A. R.; Newbold, C.; Carter, P.; Cowan, R.; Wallace, G. G., Measuring the effective area and charge density of platinum electrodes for bionic devices. *Journal of Neural Engineering* **2018,** *15* (4), 046015.
54. Harris, A. R.; Allitt, B. J.; Paolini, A. G., Predicting neural recording performance of implantable electrodes. *Analyst* **2019,** *144* (9), 2973-2983.
55. LAURENS, N.; KOOLWIJK, P.; DE MAAT, M. P. M., Fibrin structure and wound healing. *J. Thromb. Haemost.* **2006,** *4* (5), 932-939.
56. Chattopadhyay, S.; Raines, R. T., Review collagen-based biomaterials for wound healing. *Biopolymers* **2014,** *101* (8), 821-833.
57. Höök, F.; Rodahl, M.; Brzezinski, P.; Kasemo, B., Energy dissipation kinetics for protein and antibody− antigen adsorption under shear oscillation on a quartz crystal microbalance. *Langmuir* **1998,** *14* (4), 729-734.
58. Malmström, J.; Agheli, H.; Kingshott, P.; Sutherland, D. S., Viscoelastic modeling of highly hydrated laminin layers at homogeneous and nanostructured surfaces: quantification of protein layer properties using QCM-D and SPR. *Langmuir* **2007,** *23* (19), 9760-9768.
59. Hovgaard, M. B.; Rechendorff, K.; Chevallier, J.; Foss, M.; Besenbacher, F., Fibronectin adsorption on tantalum: the influence of nanoroughness. *The Journal of Physical Chemistry B* **2008,** *112* (28), 8241-8249.
60. Rechendorff, K.; Hovgaard, M. B.; Foss, M.; Zhdanov, V.; Besenbacher, F., Enhancement of protein adsorption induced by surface roughness. *Langmuir* **2006,** *22* (26), 10885-10888.
61. Laurens, N.; Koolwijk, P.; De Maat, M., Fibrin structure and wound healing. *J. Thromb. Haemost.* **2006,** *4* (5), 932-939.
62. Roach, P.; Farrar, D.; Perry, C. C., Interpretation of protein adsorption: surface-induced conformational changes. *J. Am. Chem. Soc.* **2005,** *127* (22), 8168-8173.
63. Lord, M. S.; Whitelock, J. M.; Simmons, A.; Williams, R. L.; Milthorpe, B. K., Fibrinogen adsorption and platelet adhesion to silica surfaces with stochastic nanotopography. *Biointerphases* **2014,** *9* (4), 041002.
64. Chung, M. C.-M., Stucture and function of transferrin. *Biochem. Educ.* **1984,** *12* (4), 146-154.
65. Wright, J. A.; Richards, T.; Srai, S. K., The role of iron in the skin and cutaneous wound healing. *The Importance Of Iron In Pathophysiologic Conditions* **2015**, 105.
66. Rho, K. S.; Jeong, L.; Lee, G.; Seo, B.-M.; Park, Y. J.; Hong, S.-D.; Roh, S.; Cho, J. J.; Park, W. H.; Min, B.-M., Electrospinning of collagen nanofibers: effects on the behavior of normal human keratinocytes and early-stage wound healing. *Biomaterials* **2006,** *27* (8), 1452-1461.
67. Chattopadhyay, S.; Raines, R. T., Review collagen-based biomaterials for wound healing. *Biopolymers* **2014,** *101* (8), 821-833.